



## Mass transfer and transient response time of a split-feed nanofiltration pilot unit

Samantha Jeffery-Black, Steven J. Duranceau\*

*Department of Civil, Environmental and Construction Engineering, University of Central Florida, 4000 Central Florida Boulevard, P.O. Box 162450, Orlando, FL 32816-2450, USA, Tel. +1 407 823 1440; Fax: +1 407 823 3315; email: [steven.duranceau@ucf.edu](mailto:steven.duranceau@ucf.edu) (S.J. Duranceau)*

Received 22 December 2015; Accepted 14 February 2016

### ABSTRACT

The transient response of a center-port nanofiltration membrane process was evaluated using a step-input dose of a sodium chloride solution. The pilot was configured as a two-stage, split-feed, center-port, 7:2 pressure vessel array process, where the feed water is fed to both ends of six-element pressure vessels, and permeate and concentrate streams are collected after only three membrane elements. The transient response was described as a log-logistic system with a maximum delay time of 285 s for an 85% water recovery and 267 gallon per minute feed flowrate. The log-logistic model was shown to be >98% accurate in predicting the transient response of the permeate streams. When compared with a first-order nonlinear regression model, there was no difference in the predictability of transient response when using the log-logistic model in first-stage and second-stage membrane processes. However, the log-logistic model was found to be more predictive in describing third-stage transient response by a factor of 236 over a first-order method. Furthermore, the homogeneous solution diffusion model was shown to effectively predict the permeate concentration for any transient permeate perturbation.

*Keywords:* Nanofiltration; Mass transfer; Split-feed; Transient response; Pilot plant; Homogeneous solution diffusion model; Log-logistic; Nonlinear regression

### 1. Introduction

Nanofiltration (NF) is often employed as a water softening technology due to its ability to provide superior multivalent ion removal, including calcium, magnesium, and sulfate, in addition to enhanced natural and synthetic organics removal [1–4]. Since NF is considered a more “loose” form of reverse osmosis, it offers many advantages, including a lower operating pressure, resulting in lower energy costs and a higher water flux [5,6].

Prior to constructing a full-scale treatment process, water utilities typically operate pilot units to gauge how a certain technology will react to a given water source. Pilot testing is often conducted to confirm process performance, optimize operating parameters, or verify process economics [7]. Pilot testing can also be used to conduct innovative research where results may be difficult to predict without piloting. Prior research has shown that the time required to determine the effect of a feed water concentration change can be estimated by monitoring the transient response to steady-state operations [8]. Furthermore, when

\*Corresponding author.

investigating how effectively a membrane removes feed water constituents, knowing the time required for permeate and concentrate streams to be affected by feed water changes is critical when developing sampling protocols [8].

Tracer studies could help in estimating times required to observe changes in unit operations, as they are used to study time transients that occur in treatment processes, typically intended to evaluate contact time for disinfectants [9]. However, evaluations intended to study the transient response of a permeate concentration change to a feed water change are less common. Previous transient response evaluations were based on simple first-order empirical models for prediction of perturbations to water quality changes. In this work, a log-logistic approach was used to determine the permeate response to a step input of salinity ahead of a two-stage, split-feed, center-port nanofiltration process.

## 2. Background

### 2.1. Full-scale nanofiltration plant

This research was conducted at the Town of Jupiter (Town) Water Treatment Plant (WTP), located along the southeast coast of Florida. In 2010, the Town constructed a 14.5 million gallon per day (MGD) nanofiltration plant to replace its aging lime softening (LS) facility and provide enhanced organics and hardness removal.

The Town's full-scale NF plant operates at an overall 85% recovery with first- and second-stage recoveries of 67 and 47%, respectively. The NF plant consists of five trains, each with capacities of 2,013 gallons per minute (gpm), and operates with a water flux of 14.9 gal/sfd. Stage 1 and stage 2 combine to form the total system permeate, which is comprised 80% from stage 1 permeate, and 20% from stage 2 permeate. A single train houses 486 membrane elements: 378 in stage 1 and 108 in stage 2, forming a 63:18 array, a ratio of 3.5:1. Membrane elements (NF270; DOW Filmtec) are 8" in diameter and have an area of 400 square feet, and a minimum magnesium sulfate rejection of 97%.

The Town's NF plant is unique in that it is a split-feed configuration—feed water enters and permeate exits each six-element pressure vessel on both ends, and concentrate is collected in the center, after only three elements. For this reason, to distinguish between the multiple permeate streams, permeate is referred to as being collected from the left, right, or combined permeate streams hereinafter. Interstage concentrate (referred to as second stage feed) is routed to the second stage, which follows the same flow regime as the

first stage. This configuration has provided decreased energy loss as a result of a lower osmotic pressure difference across the membrane surface. Fig. 1 illustrates the split-feed flow path and configuration, in addition to the associated nanofiltration pretreatment process.

### 2.2. Split-feed pilot unit

The split-feed pilot unit was commissioned in December 2014, and designed to replicate the existing full-scale system operated by the Town. Feed water is routed directly to the pilot after the full-scale pretreatment process, which includes sand filtration, sulfuric acid and scale inhibitor addition, and cartridge filtration. The pilot operates a feed flow at 260 gpm, with an 85% recovery, and a 7:2 array. The pilot houses a total of 54 membrane elements in 9 pressure vessels, with 42 elements in the first stage, and 12 elements in the second stage. The pilot unit uses the same membrane elements as the full-scale plant (NF270; Dow Filmtec). The calculated water flux of the pilot unit is 15.1 gal/sfd, equivalent to that of the full-scale plant.

## 3. Homogeneous solution diffusion model

The main purpose of NF modeling is to be as realistic as possible when describing the membrane process, allowing better model predictions when adjusting model parameters [6]. A majority of nanofiltration modeling research utilized only very dilute and idealized solutions, containing few ions. Models have been derived to predict the response of traditionally configured nanofiltration pilots, frequently using the Nernst-Planck equation (or modified versions of the Nernst-Planck equation), the homogeneous solution diffusion model (HSDM) or nonlinear regression [8,10–19].

The solution-diffusion model is based on the fundamental acceptance that water flux is proportional to a gradient in chemical potential [13]. In this model, constituents dissolve through the membrane down a concentration gradient, and a separation is achieved based on the amount of the constituent that dissolved in the membrane and the rate the material diffuses through the membrane [8,13]. Eqs. (1) and (2) present the water flux ( $F_w$ ) and solute flux ( $F_s$ ) in a membrane process, respectively. While the water flux is highly dependent on pressure, the solute flux is not [13]:

$$F_w = K_w(\Delta P - \Delta\pi) = \frac{Q_p}{A} \quad (1)$$

$$F_s = K_s(C_m - C_p) = K_s \left[ \left( \frac{C_f - C_c}{2} \right) - C_p \right] = \frac{Q_p C_p}{A} \quad (2)$$

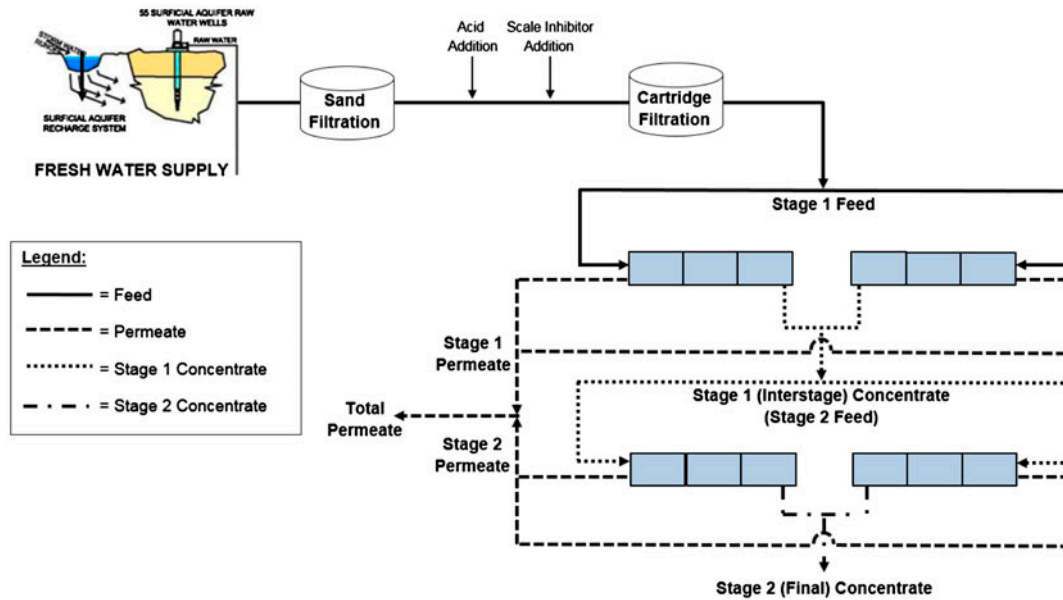


Fig. 1. Simplified schematic of the split-feed nanofiltration process.

where  $F_w$  = water flux (gpd/ft<sup>2</sup>),  $K_w$  = water mass transfer coefficient (day<sup>-1</sup>),  $\Delta P$  = transmembrane pressure differential (psi),  $\Delta\pi$  = transmembrane osmotic pressure differential (psi),  $Q_p$  = permeate flow rate (gpd),  $A$  = membrane area (ft<sup>2</sup>),  $F_s$  = solute flux (lb/ft<sup>2</sup>/d),  $K_s$  = solute mass transfer coefficient (ft/d),  $C_m$  = concentration at membrane surface (lb/ft<sup>3</sup>),  $C_p$  = permeate concentration (lb/ft<sup>3</sup>),  $C_f$  = feed concentration (lb/ft<sup>3</sup>),  $C_c$  = concentrate concentration (lb/ft<sup>3</sup>).

Both water flux and solute flux are dependent on water recovery, defined as the permeate flow rate divided by the feed flow rate, and is presented in Eq. (3):

$$R = 100 \times \frac{Q_p}{Q_f} \quad (3)$$

Once the water and solute mass transfer coefficients (MTCs) are obtained, either from the membrane manufacturer (for  $K_w$ ) or experimentally (for  $K_s$ ), Eqs. (1)–(3) in conjunction with standard mass balance equations, can be rearranged to form Eq. (4), which is used to predict permeate concentration:

$$C_p = \frac{K_s C_f}{K_w (\Delta P - \Delta\pi) \left( \frac{2-2R}{2-R} \right) + K_s} \quad (4)$$

The development of models that predict the transient response for a permeate stream has been reported elsewhere [8]. Eq. (5) was developed to predict perme-

ate concentration in a staged system where concentrate is used as feed water for succeeding stages at time infinity:

$$C_{p,\text{system}} = \frac{C_{f_i} \sum_{i=1}^n A_i K_{w_i} \Delta P_i Z_i \prod_{j=2}^i X_{j-1}}{\sum_{i=1}^n A_i K_{w_i} \Delta P_i} \quad (5)$$

#### 4. Materials and methods

Three experiments were conducted from June to September 2015 to evaluate the pilot's response to NaCl addition to the feed water. Experimental methods similar to those used by [8] were adopted, and are summarized herein. For brevity, only the methods used for experiment 3 will be discussed in detail, although the same procedures were applied to the two preceding experiments conducted in this work.

Experiment 3 was conducted on 11 September 2015. Prior to starting the experiment, pilot operating parameters (including recovery, flow rate, and pressure) and initial conductivity measurements from feed, permeate, and concentrate streams were recorded. The conductivity of the pilot feed water, which is mainly composed of multivalent ions, measured 826  $\mu\text{S}/\text{cm}$ . The conductivity in the system permeate measured 507  $\mu\text{S}/\text{cm}$ , resulting in an estimated rejection of 37.7%, which was expected given the relatively loose NF membrane (NF270). A NaCl feed solu-

Table 1  
Feed solution conductivities and recoveries operated during three experiments

Experiment no.	Conductivity in feed solution (mS/cm)	Recoveries operated (%)
1	115	80, 85
2	125	75, 80
3a	64	80, 85
3b	101	85

tion was created with a conductivity of 65 mS/cm, by adding NaCl to a bucket containing pretreated feed water. A positive displacement pump (Prominent®) was used to continuously add the salt solution to the pilot feed water stream. Prior to starting the experiments, flow tests were conducted using feed water without NaCl addition until a desired flow rate of 0.72 L/min was achieved. Since the pilot operates with a feed flow of 260 gpm (984 L/min), it was estimated that the feed water conductivity would increase to 874  $\mu$ S/cm. Assuming a rejection of 37.7%, this would result in an estimated permeate conductivity of 544  $\mu$ S/cm, enough to cause a noticeable change in permeate and concentrate conductivity. A summary of feed solution conductivities and recoveries operated is presented in Table 1. Experiment 3 is split into two sections, 3a and 3b, to distinguish between two different feed solution conductivities, although they were conducted on the same day.

Immediately after the continuous addition of the saline feed test solution to the pilot's feed water began, water samples were collected every 15 s for a period of 9 min—well after the time estimated that the pilot required to reach steady state based on previous screening evaluations. Samples were collected from stage 1, stage 2, and total permeate sample ports, including left and right sides of the pressure vessels,

where applicable. In addition, conductivity measurements for feed, first- and second-stage permeate, total system permeate, interstage concentrate (stage 2 feed), and final concentrate obtained by supervisory control and data acquisition (SCADA) were recorded by video, then later transcribed into Microsoft Excel® for subsequent analyses. Samples were also collected intermittently from feed, interstage concentrate (stage 2 feed), and final concentrate sampling ports to validate SCADA readings throughout the experiment. Table 2 presents a summary of how and when permeate conductivity measurements were obtained.

After the completion of the experiment, the conductivity of the samples was measured and recorded. To start a new experiment, the pilot water recovery was adjusted to the desired set point and allowed at least 30 min to reach steady state. The same methods were followed during the previous experiments, although the feed solutions did not always have the same conductivities, as described previously in Table 1, consequently resulting in various conductivity changes in the feed, permeate, and concentrate streams.

## 5. Results and discussion

### 5.1. Pilot response

In this work, pilot response refers to the required length of time the pilot needed to reach steady state after NaCl was added to the feed water, and how the pilot reacted when feed water chemistry changed. Table 3 presents a summary of conductivity measurements, increases, and salt rejection during experiments. The initial feed conductivity in experiments 1, 2, and 3 ranged from 810 to 836  $\mu$ S/cm. After the addition of the NaCl solution was initiated, the feed conductivity increased anywhere in the range of 6.1–12%. Initial permeate conductivity measurements ranged from 483  $\mu$ S/cm in the lower recovery

Table 2  
Summary of data collection procedures

Sample stream	Manually collected	SCADA
Feed	Intermittently	Every 5 s
Stage 1 permeate left	Every 15 s	Never
Stage 1 permeate right	Every 15 s	Never
Stage 1 permeate combined	Every 15 s	Every 5 s
Interstage concentrate (stage 2 feed)	Intermittently	Every 5 s
Stage 2 permeate left	Every 15 s	Never
Stage 2 permeate right	Every 15 s	Never
Stage 2 permeate combined	Every 15 s	Every 5 s
Total system permeate	Every 15 s	Every 5 s
Final concentrate	Intermittently	Every 5 s

Table 3  
Conductivity measurements in feed and permeate streams at various water recoveries

Experiment no.	Recovery (%)	Initial feed conductivity ( $\mu\text{S}/\text{cm}$ )	Steady-state feed conductivity ( $\mu\text{S}/\text{cm}$ )	Increase in feed conductivity (%)	Initial total permeate conductivity ( $\mu\text{S}/\text{cm}$ )	Steady-state total permeate conductivity ( $\mu\text{S}/\text{cm}$ )	Increase in total permeate conductivity (%)	Initial salt rejection (%)	Steady-state salt rejection (%)
1	80	836	889	6.3	483	534	11	42	40
2	85	836	889	6.3	510	554	8.6	39	38
	75	810	862	6.4	501	547	9.2	38	37
3a	80	837	888	6.1	483	534	11	42	40
	85	836	889	6.3	510	554	8.6	39	38
	75	825	888	7.6	494	549	11	40	38
	80	825	880	6.7	494	545	10	40	38
3b	85	825	885	7.3	510	559	9.6	38	37
	85	824	907	10.1	507	586	16	38	35

Notes: 3a and 3b were conducted on the same day, but with different NaCl concentrations in the feed solution.

Table 4

Response time (seconds) during experiments 1, 2, and 3 at 85% recovery

Permeate stream	Experiment 1	Experiment 2	Experiment 3
1st stage	180	195	165
2nd stage and total system	285	255	255

experiments to 510  $\mu\text{S}/\text{cm}$  in the experiments conducted at a higher water recovery, as expected. At a certain time after NaCl addition began, the permeate stream reached a steady conductivity value, ranging from 534 to 586  $\mu\text{S}/\text{cm}$ , with lower values observed in lower water recoveries, and higher values measured in higher water recoveries, as would be expected. This resulted in an increased total system permeate conductivity increase ranging from 8.6 to 19%.

Table 4 presents the response times of the first-stage, second-stage, and total system permeate streams. The first-stage permeate stream reached a steady conductivity value after 165 (2 min, 45 s)–195 s (3 min, 15 s), while second-stage and total system permeate reached a steady conductivity value after 255 s (4 min, 15 s)–285 s (4 min, 45 s).

In figures illustrating conductivity as a function of time (Figs. 2 through 6), there appears to be a lag from when NaCl is first in contact with the permeate stream to when the stream achieves steady state with respect to NaCl concentration. For example, in Fig. 2, during the time between 50 and 165 s the conductivity gradually increases, indicating NaCl diffusion. It is suspected that this gradual increase is caused from axial dispersion within the pilot pipes and appurtenances.

Figs. 2, 3, and 4 illustrate first-stage, second-stage, and total system permeate conductivities at 85 and 80% water recoveries during experiment 3a, respectively. As would be expected, the permeate streams have a higher conductivity throughout the experiment conducted at 85%, compared to the experiment conducted at 80% recovery. Based on these results, it appears that changing the recovery does not significantly affect the response time of the permeate, or how long it takes for the permeate stream to be affected by changes in feed water chemistry. However, changing the recovery does impact the conductivity measured in the permeate streams

Fig. 5 depicts a graphical summary of experiment 3a. In this figure, stage 1 permeate conductivity is illustrated in dark gray, stage 2 permeate conductivity measurements are depicted in black, and total permeate conductivity is shown using light gray symbols. It is important to note that stage 1 and total system permeate conductivities are plotted on the right axis to

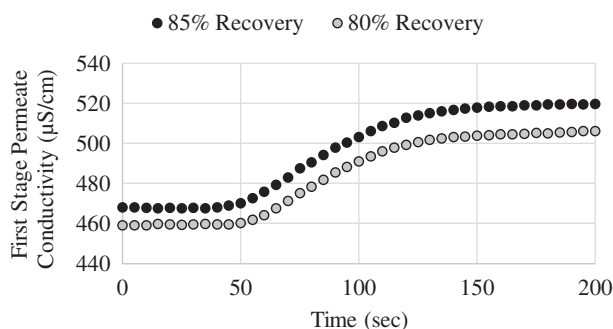


Fig. 2. First-stage permeate conductivity at 85 and 80% recoveries.

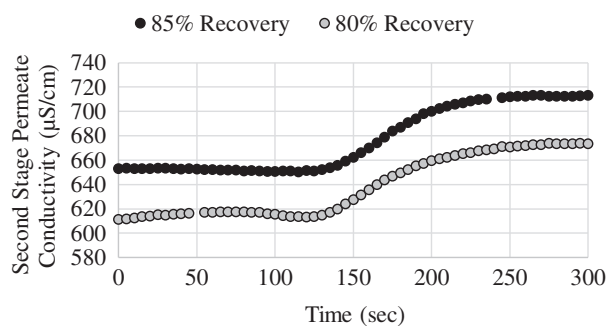


Fig. 3. Second-stage permeate conductivity at 85 and 80% recoveries.

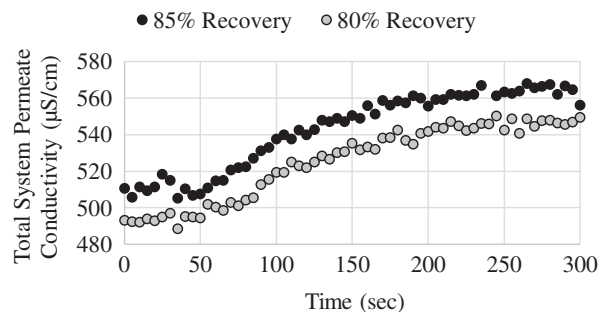


Fig. 4. Total pilot permeate conductivity at 85 and 80% recoveries.

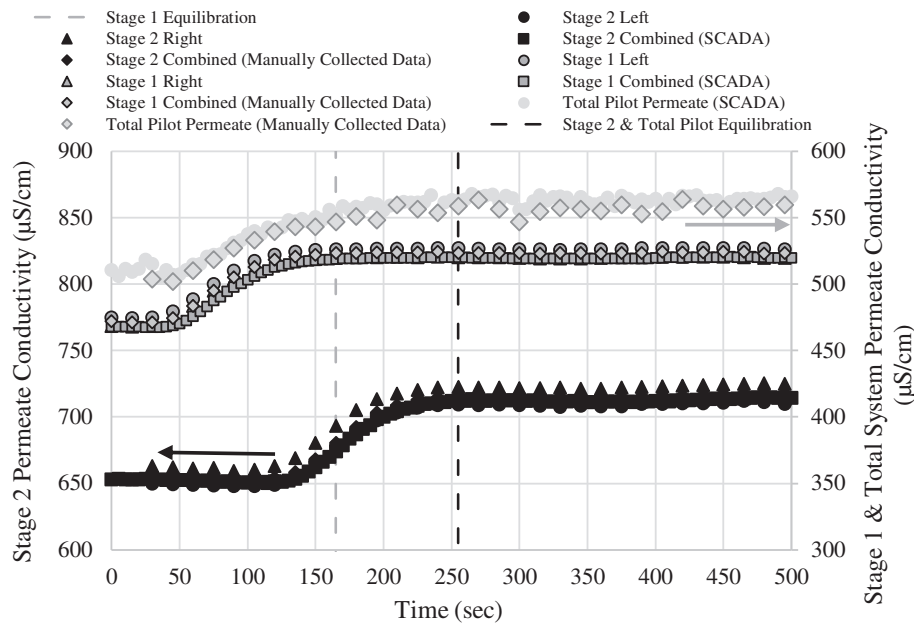


Fig. 5. Pilot response at 85% recovery.

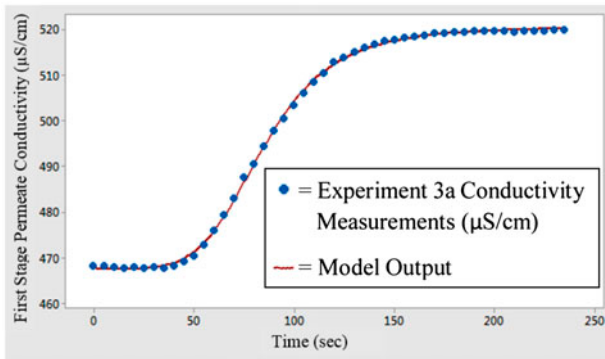


Fig. 6. Minitab® figure describing first-stage permeate conductivity vs. time.

allow for easier comparison with stage 2 conductivity. Based on these results, it appears that manually collected data and data obtained from the SCADA output agree closely with one another. In Fig. 5, it is easier to compare how various permeate streams respond to NaCl addition to the feed water. First-stage permeate conductivity begins to increase first, followed by total permeate conductivity. However, total conductivity does not stabilize until second-stage permeate conductivity since total permeate is comprised of both first- and second-stage permeates.

5.1.1. Predictive modeling

Logistic nonlinear regression equations are utilized to describe sigmoidal growth curves [19,20]. In this

Table 5  
Minitab® model statistics summary

Statistic	Experiment 2, 85% recovery			Experiment 3, 85% recovery		
	First stage	Second stage	Total system	First stage	Second stage	Total system
Iterations	10	8	8	7	8	12
SSE	13.8	10.4	131.3	9.89	60.3	437
DF	12	22	22	43	52	52
MSE	1.15	0.473	5.97	0.230	1.16	8.40
s	1.07	0.687	2.44	0.480	1.08	2.90
Model end time (sec)	240	555	555	235	285	285

Notes: SSE = sum of square error; DF = degrees of freedom; MSE = mean square error; s = standard deviation.

Table 6  
Theta values for permeate log-logistic models at 85% recovery

Parameter	Experiment 2, 85% recovery			Experiment 3, 85% recovery		
	First stage	Second stage	Total system	First stage	Second stage	Total permeate
$\theta_1$	509	694	552	521	713	567
$\theta_2$	461	634	499	467	652	509
$\theta_3$	111	206	137	84.6	175	110
$\theta_4$	4.74	5.63	3.82	4.89	10.4	3.32

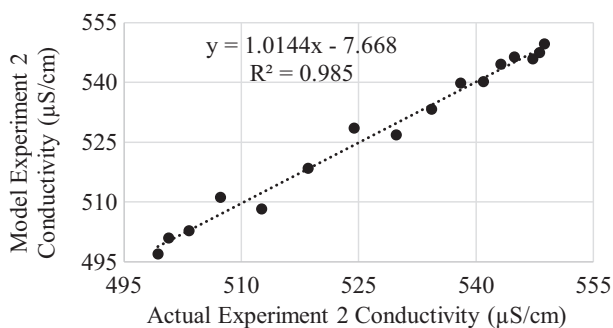


Fig. 7. Model (experiment 2) vs. actual data (experiment 2).

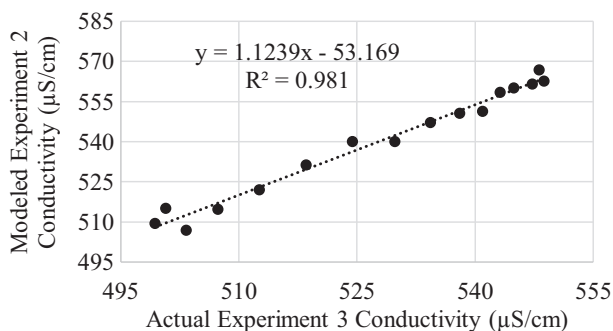


Fig. 8. Model (experiment 2) vs. actual data (experiment 3).

work, an adaptation of the logistic model, the log-logistic model, was utilized to determine the response of permeate streams after NaCl addition, and it is presented in Eq. (6). This model is frequently used in bioassay work to determine dose–response curves and has also been used to model water demand data [21,22]:

$$\text{Predicted Concentration at time, } t: \theta_1 + \frac{\theta_2 - \theta_1}{\left[1 + \exp\left(\theta_4 \ln \frac{t}{\theta_3}\right)\right]} \quad (6)$$

where  $\theta_1$  = parameter describing upper boundary of conductivity measurements,  $\theta_2$  = parameter describing lower boundary of conductivity measurements,  $\theta_3$  = parameter describing time (sec) needed to reach conductivity halfway between upper and lower boundaries,  $\theta_4$  = parameter describing slope of increase in conductivity,  $t$  = time (sec).

An example of how Eq. (6) was used in this research is demonstrated using Fig. 6, which depicts the Minitab<sup>®</sup> output model for the first-stage permeate stream at 85% recovery. In Fig. 6, data from experiment 3a were used and are plotted in blue dots, while the red line represents the model. Tables 5 and 6 present the Minitab<sup>®</sup> model statistics and the theta values obtained, respectively. The models summarized in Tables 5 and 6 were generated from first-stage, second-stage, and total pilot permeate response during experiments 2 and 3. In general, as the sum of the square error (SSE) and thus the mean square error (MSE) become lower, a model is more acceptable. The model generated and illustrated in Fig. 6 has an SSE and MSE of 9.89 and 0.230, respectively. Of the six models summarized in Table 5, the model presented in Fig. 6 (first-stage permeate response, experiment 3a) provides the most accurate representation of transient response time.

Figs. 7 and 8 illustrate how accurately the modeled data represent actual total system permeate response. In Figs. 7 and 8, the vertical axis represents the modeled data from experiment 2, while the horizontal axes represent raw data from experiments 2 and 3, respectively. Figs. 7 and 8 only include data during the time in which conductivity is increasing, 45–285 s. In Fig. 7, the  $R^2$  value of 0.985 indicates the predicted conductivity measurements predicts 98.5% of the actual conductivity data. Fig. 8 illustrates experiment 2 predicted data vs. experiment 3 actual data, and the  $R^2$  value was calculated as 0.981, indicating the modeled data predicts 98.1% of experiment 3 data.

To compare the log-logistic model with a first-order nonlinear regression model presented in Eq. (5),

Table 7  
Minitab® model and statistics summary and theta values

Statistic/Parameter	First stage	Second stage	Third stage
Iterations	13	24	11
DF	13	13	13
MSE	0.136	0.821	0.0530
s	0.369	0.906	0.230
$\theta_1$	13.9	22.4	21.6
$\theta_2$	4.08	4.87	6.90
$\theta_3$	1.59	2.28	2.04
$\theta_4$	7.98	4.10	5.98

Table 8  
Comparison between first-order and log-logistic models

Statistic	First stage		Second stage		Third stage	
	First-order	Log-logistic	First-order	Log-logistic	First-order	Log-logistic
SSE	1.4	1.8	10.9	10.8	161.8	0.6873

Notes: First-order SSE values obtained from [8].

Table 9  
Solute flux (lb/sfd)

Stage/System	Solute flux (lb/sfd)			
	Chloride	Sodium	TDS	Sulfate
1st stage	0.0070	0.0026	0.045	0.0004
2nd stage	0.0081	0.0034	0.063	0.0006
Total system	0.0072	0.0027	0.048	0.0005

Table 10  
MTCs (ft/d)

Constituent	Mass transfer coefficients (ft/d)
Chloride	10.4
Sodium	2.14
TDS	0.872
Sulfate	0.0150

chloride data obtained from early transient response work using a three-stage nanofiltration pilot process were used [8]. Statistical results and theta values generated using the log-logistic equation (Eq. (4)) Minitab® are presented in Table 7.

Table 8 provides a comparison between statistical SSE values from first-order and log-logistic models. First-order SSE values were obtained directly from [8]. SSE values are used to describe the error of the model, meaning the larger the SSE, the more error the model

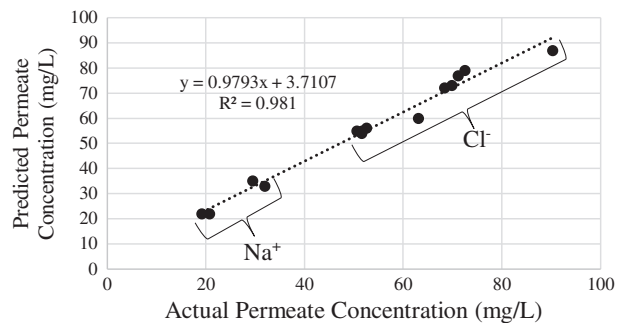


Fig. 9. Predicted vs. actual permeate sodium and chloride concentrations.

produces; consequently, a lower SSE value indicates a better-fit model. Comparing values in Table 8, it appears that the first-order models are a better fit for stage 1 and stage 2 permeate streams, although the log-logistic model is still acceptable based on Table 7 statistics. In regards to stage 3 response time, the log-logistic model is a significantly better fit, where the first-order model provides an SSE of 161.8, and the log-logistic model provides an SSE of 0.6873.

## 5.2. Homogeneous solution diffusion model

The HSDM, presented previously in Eqs. (1)–(4), can be used to predict permeate concentrations, given water and solute MTCs, transmembrane pressure, and

osmotic pressure differential values. In this work, the HSDM was used to predict the concentration of sodium and chloride in the permeate streams. Solute flux and MTCs for various constituents evaluated in pilot sampling are presented in Tables 9 and 10, respectively. These values were calculated based on pilot start-up data obtained prior to the transient response experiments. Solute flux in the total system permeate stream (lb/sfd) ranges from 0.0005 for sulfate to 0.048 for total dissolved solids (TDS). MTCs (ft/day) range from 0.0150 for sulfate to 10.4 for chloride.

The values presented in Tables 9 and 10 were used in Eq. (4) to predict permeate sodium and chloride concentrations prior to NaCl addition, and after permeate streams reached steady state upon NaCl addition. Fig. 9 depicts the predicted vs. actual sodium and chloride concentrations obtained from first-stage, second-stage, and total system permeate streams during multiple experiments conducted at an 85% recovery. Data obtained using the predictive diffusion model presented in Eq. (4) are able to predict 98.1% of sodium and chloride permeate concentrations accurately.

## 6. Conclusions

The purpose of this research was to monitor time transients that occurred in the permeate concentration of a two-stage, split-feed, center-port membrane process after a change in the feed water content was induced. The time required for first-stage, second-stage, and total system permeate streams to observe an effect in feed water changes was delineated and modeled using a log-logistic nonlinear regression equation. Total system permeate required between 255 and 285 s to reach steady state, as demonstrated during three repetitive experiments. Using a safety factor of three, it was determined that the system should be allowed to operate for at least 14 min and 15 s prior to sampling each process stream for chemical analysis.

When compared with a first-order nonlinear regression model, there was no difference in the predictability of transient response when using the log-logistic model in first-stage and second-stage membrane processes. However, the log-logistic model was found to be more predictive in describing a previously studied [8] third-stage transient response by a factor of 236 over a first-order method. Furthermore, the HSDM was shown to effectively predict the permeate concentration for any transient permeate perturbation.

## Acknowledgments

The work reported herein was funded by Jupiter Water Utilities (Jupiter), FL using a cooperative agreement via a contract between Kimley-Horn & Associates, Inc. (KHA) and the University of Central Florida (UCF) through agreement number 16208114. Any opinions, findings, and conclusions expressed in this material are those of the authors and do not necessarily reflect the view of UCF (Orlando, FL), its Research Foundation nor KHA and Jupiter, FL. The authors acknowledge the Jupiter's staff, including D. Brown, A. Barnes, P. Jurczak, and R. Wilder, for their assistance and support, without whom this work would not have been possible. The advice of I. Watson (RosTek Associates Inc., Tampa, FL) and J. Potts (Kimley-Horn & Associates, Inc., West Palm Beach, FL) were appreciated and hereby noted. The contributions of UCF graduate and undergraduate students who assisted in field and laboratory work are deeply appreciated (C. Higgins, J. Ousley, S. Myers, C. Conover, M. Arenas, M. Coleman, A. Netcher, P. Biscardi and D. Yonge).

## References

- [1] W.J. Conlon, S.A. McClellan, Membrane softening: A treatment process comes of age, *J AWWA* 81(11) (1989) 47–51.
- [2] T.J. Blau, J.S. Taylor, K.E. Morris, L.A. Mulford, dbp control by nanofiltration: Cost and performance, *J. AWWA* 84(12) (1992) 104–116.
- [3] United States Environmental Protection Agency, ICR Manual for Bench- and Pilot-scale Treatment Studies, EPA 814/B-96-003, Washington, DC, 1996.
- [4] S.J. Duranceau, J.S. Taylor, SOC removal in a membrane softening process, *J. AWWA* 84(1) (1992) 68–78.
- [5] N. Hilal, H. Al-Zoubi, N.A. Darwish, A.W. Mohammad, M. Abu Arabi, A comprehensive review of nanofiltration membranes: Treatment, pretreatment, modelling, and atomic force microscopy, *Desalination* 170 (2004) 281–308.
- [6] A.W. Mohammad, Y.H. Teow, W.L. Ang, Y.T. Chung, D.L. Oatley-Radcliffe, N. Hilal, Nanofiltration membranes review: Recent advances and future prospects, *Desalination* 356 (2015) 226–254.
- [7] M. Wilf, *The Guidebook to Membrane Desalination Technology*, Balaban Desalinations Publications, Hopkinton, MA, 2011.
- [8] S.J. Duranceau, Modeling the permeate transient response to perturbations from steady state in a nanofiltration process, *Desalin. Water Treat.* 1 (2009) 7–16.
- [9] S. Teefy, *Tracer Studies in Water Treatment Facilities: A Protocol and Case Studies*, Water Research Foundation, Denver, CO, 1996.
- [10] K. Wesolowska, S. Koter, M. Bodzek, Modelling of nanofiltration in softening water, *Desalination* 162 (2004) 137–151.

- [11] Y. Roy, M.H. Sharqawy, J.H. Lienhard, Modeling of flat-sheet and spiral-wound nanofiltration configurations and its application in seawater nanofiltration, *J. Membr. Sci.* 493 (2015) 360–372.
- [12] S.J. Duranceau, Doctoral Dissertation, University of Central Florida, Orlando, FL, 1990.
- [13] J.G. Wijmans, R.W. Baker, The solution-diffusion model: A review, *J. Membr. Sci.* 107 (1995) 1–21.
- [14] T. Chaabane, S. Taha, M. Taleb Ahmed, R. Maachi, G. Dorange, Coupled model of film theory and the Nernst–Planck equation in nanofiltration, *Desalination* 206 (2007) 424–432.
- [15] R. Schlögl, Membrane permeate in system far from equilibrium, *Berichte der Bunsengesellschaft Physik. Chem.* 70 (1966) 400–414.
- [16] L. Dresner, Some remarks on the integration of the extended Nernst–Planck equations in the hyperfiltration of multicomponent solutions, *Desalination* 10 (1972) 27–46.
- [17] A.L. Ahmad, B.S. Ooi, Characterization of composite nanofiltration membrane using two-parameters model of extended Nernst–Planck equation, *Sep. Purif. Technol.* 50 (2006) 300–309.
- [18] W.R. Bowen, H. Mukhtar, Characterisation and prediction of separation performance of nanofiltration membranes, *J. Membr. Sci.* 112 (1996) 263–274.
- [19] Y. Garba, S. Taha, N. Gondrexon, G. Dorange, Ion transport modelling through nanofiltration membranes, *J. Membr. Sci.* 160 (1990) 187–200.
- [20] G.A.F. Seber, C.J. Wild, *Nonlinear Regression*, John Wiley & Sons Inc., New York, NY, 1989.
- [21] J.C. Streibig, P. Kudsk, *Herbicide Bioassays*, CRC Press, Boca Raton, FL, 1993.
- [22] S. Surendran, K. Tota-Maharaj, Log logistic distribution to model water demand data, *Procedia Eng.* 119 (2015) 798–802.